A Coarse-Grained Description of Star−Linear Polymer Mixtures

Christian Mayer* and Christos N. Likos

Institut für Theoretische Physik II: Weiche Materie, Heinrich-Heine-Universität Düsseldorf, Universitätsstrasse 1, D-40225 Düsseldorf, Germany

Received September 12, 2006; Revised Manuscript Received November 27, 2006

ABSTRACT: We put forward a scheme for bridging the length and time scales for soft composite materials consisting of high functionality star polymers and chemically identical polymer chains of smaller size, dissolved into a good or athermal solvent. By employing monomer-level computer simulations and invoking arguments from scaling and Flory theory, we derive realistic effective interactions between the star centers and the midpoint of the chains, which are used as effective coordinates for the mesoscopic description of such mixtures. On the basis of these interactions, we analyze the macroscopic behavior of the same, finding good agreement with previously published experimental results regarding the structure and rheology of this novel type of composite materials. The added chains lead to cluster formation between the stars in a dilute star solution and bring about melting of the star glass at high concentrations of the same. An intriguing insensitivity of the chain-modified star−star effective interaction on the linear polymer concentration is discovered, and the implications of this property are critically discussed.

I. Introduction

Soft, composite materials are physical systems of great theoretical interest and enormous potential technological relevance. Probably the simplest such system that has been extensively studied is a mixture between hard, impenetrable colloids and nonadsorbing polymer chains, which features an extremely rich phenomenology, both in and out of equilibrium.[1,2] In model colloid−polymer mixtures, all the physics is dictated by entropy: the colloids are modeled as hard spheres and the polymers as self-avoiding chains;[3] thus, all effective interactions scale linearly with thermal energy. Most of the physics of colloid−polymer mixtures can be captured by the depletion mechanism, which amounts to the fact that two colloids brought at a surface-to-surface distance smaller than the polymer size are pushed together by the unbalanced osmotic pressure of the polymer solution. This allows for the modeling of colloids in a polymer bath as "sticky spheres".

In colloid−polymer mixtures, the crucial physical characteristic that dictates the quantitative features of the depletion attraction is the impenetrability of the colloids to the polymers as well as the hard-sphere character of the colloid−colloid interaction itself. A whole new range of possibilities to tune and steer the behavior of composite materials arises when the hard colloids are replaced by soft ones. One example are charge-stabilized colloidal mixtures, which can be modeled as Yukawa mixtures with varying amplitudes and decay lengths.[4] Another example of soft colloids are star polymers with f arms (functionality), which display enormous richness in their equilibrium and rheological properties.[5,6] Adding homopolymer chains in a star polymer mixture is a process that can bring about drastic changes in the behavior of the solution in a well-defined way: the partial concentrations of the two components, the functionality f, and the linear-to-star polymer size ratio are experimental quantities that can be accurately controlled. In this work, we present a coarse-grained description of such mixtures, based on the derivation and application of effective interactions. We coarse-grain the chains around their mid-monomer and the stars around their center and develop an accurate theoretical model for the star−chain interaction, whose validity is confirmed by comparison with computer simulations. We analyze the salient properties of star−linear mixtures on the basis of the effective interactions, focusing on cluster formation and rheology control (glass melting through polymer additives).

The rest of this paper is organized as follows. In section II we discuss the effective interactions between particles of the same species, and in section III we present the simulation and theoretical approaches to derive accurate effective interactions between unlike species for arbitrary star functionalities and size ratios. In section IV we turn then our attention to the study of the properties of many-body star−linear mixtures, based on the coarse-grained interactions introduced before. We analyze the effect of the chains on the star structure and dynamics at the two extremes: low and high star concentration. Finally, in section V we summarize and draw our conclusions.

II. Star−Star and Chain−Chain Interactions

The strategy employed throughout this work is that of *coarse-graining* of both components, the stars and the linear chains (coded with the subscripts "s" and "c", respectively, in what follows.) In this approach, which enables us to form a bridge between the microscopic and the mesoscopic scales, suitable coordinates that characterize the star and the chain as a whole are chosen, and all the remaining fluctuations of the monomers are traced out in a well-defined statistical mechanical fashion.[7] In particular, the effective coordinates are kept fixed in any prescribed configuration, and the restricted, canonical partition function of all the remaining ones is (approximately) calculated. To simplify the situation, suppose that we are having only two mesoscopic particles (regardless of their type) in the system and let $r_{1,2}$ denote the *fixed* position vectors of their respective effective coordinate. Denote as $\mathcal{Z}_{\alpha\beta}(\mathbf{r}_1,\mathbf{r}_2)$ the aforementioned restricted partition function, where α,β = c,s. The quantity of interest is then the effective interaction $V_{\alpha\beta}(\mathbf{r}_1,\mathbf{r}_2)$, defined as

$$V_{\alpha\beta}(\mathbf{r}_1,\mathbf{r}_2) = -k_B T \ln\left[\frac{\mathcal{Z}_{\alpha\beta}(\mathbf{r}_1,\mathbf{r}_2)}{\mathcal{Z}_{\alpha\beta}(|\mathbf{r}_1 - \mathbf{r}_2| \to \infty)}\right] \qquad (1)$$

with Boltzmann's constant k_B and the absolute temperature T. We also define here $\beta = (k_B T)^{-1}$ for future reference. In other

10.1021/ma062117z CCC: $37.00
Published on Web 01/17/2007

words, the effective interaction is the free energy cost for bringing the two particles from infinity to their prescribed positions $\mathbf{r}_1$ and $\mathbf{r}_2$. When averaging over all but a single effective coordinate of a macromolecule and there are only two such present, we have $V_{\alpha\beta}(\mathbf{r}_1,\mathbf{r}_2) = V_{\alpha\beta}(r)$, where $r = |\mathbf{r}_1 - \mathbf{r}_2|$. In general, many-body effective terms result from the process of coarse-graining, but they are ignored in the pair-potential approximation. In a system containing $\mathcal{N}_s$ stars and $\mathcal{N}_c$ chains, the total effective potential energy U reads then as

$$U = \sum_{i<j}^{\mathcal{N}_s}\sum_{j=1}^{\mathcal{N}_s} V_{ss}(|\mathbf{r}_i - \mathbf{r}_j|) + \sum_{i<j}^{\mathcal{N}_c}\sum_{j=1}^{\mathcal{N}_c} V_{cc}(|\mathbf{r}_i - \mathbf{r}_j|) + \sum_{i=1}^{\mathcal{N}_s}\sum_{j=1}^{\mathcal{N}_c} V_{sc}(|\mathbf{r}_i - \mathbf{r}_j|) \quad (2)$$

Hence, both species, stars and chains, are figured as soft spheres interacting with the corresponding soft potentials $V_{\alpha\beta}(r)$.

The natural question that arises is, which coordinates should be chosen as effective ones? For the star polymers, and in particular in the case of high functionality f, the position of their central particle, on which all chains are grafted, is the natural one. The corresponding effective interaction V_{ss} has been derived a long time ago,[8,9] and its validity has been confirmed through extensive comparisons with scattering data[9,10] and computer simulations.[11] It reads as[9]

$$\beta V_{ss}(r) = \frac{5}{18} f^{3/2} \times \begin{cases} -\ln\left(\frac{r}{\sigma_s}\right) + \frac{1}{1+\sqrt{f}/2} & \text{for } r \le \sigma_s \\ \frac{1}{1+\sqrt{f}/2}\frac{\sigma_s}{r}\exp\left[-\frac{\sqrt{f}}{2\sigma_s}(r-\sigma_s)\right] & \text{else} \end{cases} \quad (3)$$

Here, σ_s is the corona diameter of the star. The distance $\sigma_s/2$ marks the crossover between the inner part of the macromolecule, where the latter resembles a semidilute polymer solution and the outer part, in which loose chains form a local, dilute solution.[9] The Yukawa part of the interaction decays with the characteristic length $2\sigma_s/\sqrt{f}$, set by the diameter of the outermost star blob. Monomer-resolved computer simulations have shown that the relation $\sigma_s \cong 4/3R_g^{(s)}$ holds, where $R_g^{(s)}$ is the radius of gyration of the star polymer.

The choice of the effective coordinate for the linear chains is less obvious. At least three possibilities have been employed repeatedly in the literature. Witten and Pincus[8] considered the coordinate of the end monomer as an effective one that characterizes the whole chain. In computer simulations[12−19] and field-theoretical approaches[12] the polymer's center of mass is an often-used coordinate, resulting into a Gaussian effective interaction of strength $\sim 2k_BT$ and range set by the chain's radius of gyration, $R_g^{(c)}$. Finally, another alternative is given by choosing the central monomer as an effective coordinate, a choice that is more symmetric than that of the end monomer.[12,20] The latter choice establishes a certain symmetry between multiarm star polymers and linear chains, since a chain of polymerization N_c now becomes equivalent to a star of functionality $f = 2$ and polymerization $N_c/2$ per arm. Accordingly, this is the choice we follow throughout this work. In this representation, the effective interaction between the polymer chains has been calculated by theory and simulation in ref 20. The interaction energy between two polymer chains as a function of the distance r between their central monomers is given by

$$\beta V_{cc}(r) = \frac{5}{18}2^{3/2}\begin{cases} -\ln\left(\frac{r}{\sigma_c}\right) + \frac{1}{2\tau^2\sigma_c^2} & \text{for } r \le \sigma_c \\ \frac{1}{2\tau^2\sigma_c^2}\exp[-\tau^2(r^2-\sigma_c^2)] & \text{else} \end{cases} \quad (4)$$

As for multiarm stars, the scale σ_c satisfies the relation[20] $\sigma_c = 4/3R_g^{(c)}$. The parameter τ is given by $\tau\sigma_c = 1.03$, a choice that guarantees the correct value of the second virial coefficient of a polymer solution.[20] The similarity between high-f ($f \gtrsim 10$) stars and linear chains ($f = 2$) is manifest by comparing the interactions of eqs 3 and 4. Both feature a logarithmic divergence for close approaches, scaling with the prefactor $(5/18)f^{3/2}$. This feature arises from general scaling considerations, as will be demonstrated shortly. However, the type of decay for larger separations is different: a Yukawa-type decay holds for multiarm stars, whereas a Gauss-type decay is valid for linear chains. The physical reason for this difference lies in the fact that high-f stars feature geometric blobs in their exterior, which arise from the crowding of the f chains in a sphere. The size of the outermost blob sets the scale for the decay of the Yukawa part of the potential.[9] Such blobs are absent in linear chains, and the interaction decays in a different way, which is much better modeled by a Gaussian.[20]

Evidently, it remains to specify the cross-interaction $V_{sc}(r)$ in order to have a full, mesoscopic description of the mixture. In refs 23−25, in which star−chain mixtures have also been considered, the approach of using the chain's center of mass as effective coordinate has been adopted. Accordingly, the chain−chain interaction was modeled by a Gaussian,[19] and for the cross-interaction a heuristic power-law form with additive length scale was assumed. That modeling led to a satisfactory description of experimental observations. Here, however, we aim at a realistic modeling of the cross-interaction, and thus a more detailed analysis is necessary, also in view of the fact that a different effective coordinate (the central monomer) is used to coarse-grain the linear polymer. This is the subject of the following section.

III. Star−Chain Interactions

A. Molecular Dynamics Simulations. One strategy leading to the determination of the unknown interaction $V_{cs}(r)$ is to employ computer simulations. These also serve as a stringent test for theoretical approximations. Computer simulations are, at the same time, limited by the degree of polymerization N and the star functionality f that can be simulated. For this purpose, we limited ourselves to moderate values of these parameters and subsequently compared the simulation results with those from theory. The excellent agreement between the two allows us then to apply the theoretical approach to arbitrary star functionalities.

We performed molecular dynamics (MD) simulations in which each monomer is resolved and calculated the effective force $F_{sc}(r)$ acting on the star center in the presence of a chain whose own central monomer is held at distance r from the former; clearly, $\mathbf{F}_{cs}(r) = -\mathbf{F}_{sc}(r)$, and the relation to $V_{sc}(r)$ reads as

$$\mathbf{F}_{cs}(r) = -\frac{\partial V_{sc}(r)}{\partial r}\hat{\mathbf{r}} \quad (5)$$

Table 1. List of the Parameters of the Simulated Systems[a]

f	N_s	N_c	$R_g^{(s)}/\sigma_{LJ}$	$R_g^{(c)}/\sigma_{LJ}$	σ_s/σ_{LJ}	σ_c/σ_{LJ}	R_d/σ_{LJ}
20	50	40	11.6	4.36	15.46	5.82	0.5
35	50	40	12.6	4.36	16.8	5.82	0.5
50	100	200	20.2	11.9	27	15.8	0.5
100	50	200	15.1	11.9	20.1	15.8	0.8

[a] The corona diameters σ_α (α = s,c) were taken to be 4/3 of the respective radii of gyration, $R_g^{(\alpha)}$, as discussed in the text.

where we position the star at the origin and the mid-monomer of the chain at $\mathbf{r} = r\hat{\mathbf{r}}$. The simulation model employed is the same used in various previous studies of star polymers and polymer chains.[11,21] In order to mimic good solvent conditions, all monomers interact with each other via a purely repulsive and truncated Lennard-Jones potential, namely

$$V_{LJ}(r) = \begin{cases} 4\epsilon\left[\left(\frac{\sigma_{LJ}}{r}\right)^{12} - \left(\frac{\sigma_{LJ}}{r}\right)^{6} + \frac{1}{4}\right] & \text{for } r \le 2^{1/6}\sigma_{LJ} \\ 0 & \text{else} \end{cases} \quad (6)$$

Here, σ_{LJ} is the monomer size and ϵ sets the energy scale. As in previous simulations,[11] we use $k_BT = 1.2\epsilon$. The monomer mass m is also taken as unitary, setting thereby the time scale of the MD simulation as $\tau_{MD} = (m\sigma_{LJ}^2/\epsilon)^{1/2}$. Connected monomers along each star arm and along the chain experience an additional bonding interaction, expressed by the finite extensible nonlinear elastic potential (FENE):

$$V_{FENE}(r) = \begin{cases} -15\epsilon\left(\frac{R_0}{\sigma_{LJ}}\right)^2 \ln\left[1 - \left(\frac{r}{R_0}\right)^2\right] & \text{for } r < R_0 \\ \infty & \text{else} \end{cases} \quad (7)$$

where $R_0 = 1.5\sigma_{LJ}$.

Because of the high monomer concentration in the center of the star, a hard core with radius R_d is introduced.[11] The interaction between the core and the monomers is the same as between the monomers, but shifted by a distance R_d of microscopic order; all parameters are summarized in Table 1. The effective force $\mathbf{F}_{sc}(r)$ above is then simply the average over all microscopic forces acting on the center of the star.[7,11] We simulated three different pairs consisting of one star and one chain; the parameter combinations are given in Table 1. The equations of motion were integrated using a time step $\Delta t = 2 \times 10^{-3}\tau_{MD}$. For every different separation r, the system was first equilibrated during 10^6 timesteps, and up to an additional 5×10^7 timesteps were used to gather the statistics. During equilibration, we couple the system to a heat bath[22] that acts as a thermostat, which is switched off at the end of equilibration time. A typical simulation snapshot is shown in Figure 1. The results from the MD simulations will be discussed in what follows, in conjunction with the theoretical modeling.

B. Theory of the Star−Linear Effective Interaction. In developing a theoretical approach for the unknown quantity $V_{sc}(r)$, two different regimes for the interparticle separation r must be considered. When the two are sufficiently close together, $r \lesssim (\sigma_s + \sigma_c)/2$, analytical considerations from scaling theory can be employed. We denote this range of separations as the scaling regime, whereas the domain $r \gtrsim (\sigma_s + \sigma_c)/2$ defines the weak overlap regime.

1. The Scaling Regime. In the scaling regime, we can invoke arguments from scaling theory.[26] The partition function $\mathcal{Z}_1$ of a linear chain with N monomers scales as

$$\mathcal{Z}_1(N) \sim z^N N^{-\nu\eta_2} \quad (8)$$

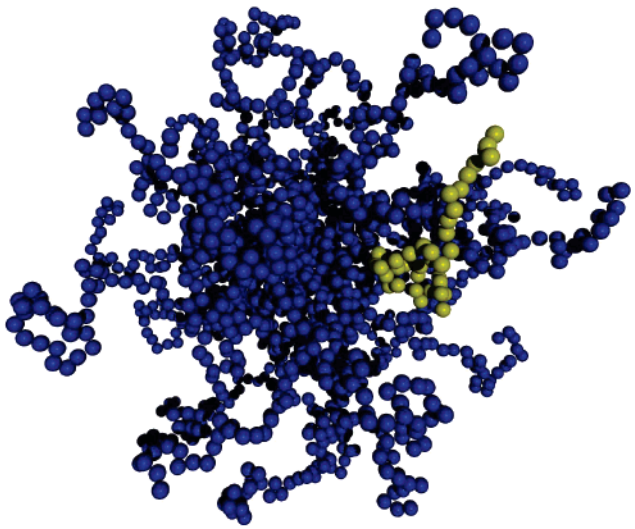

Figure 1. Simulation snapshot of a star polymer with $f = 35$ arms and $N_s = 50$ monomers (dark beads) per chain and a linear chain with $N_c = 40$ monomers (light gray beads) at a center-to-center distance $r = 10\sigma_{LJ}$.

where the fugacity z is a quantity depending on microscopic details, but the Flory exponent $\nu \cong 3/5$ and the exponent η_2 are universal for all polymers in good solvent conditions. Equation 8 can be generalized to f-arm stars and reads as

$$\mathcal{Z}_f(N) \sim z^{fN} N^{\nu(\eta_f - f\eta_2)} \quad (9)$$

with the family of exponents η_f being known from renormalization group analysis and simulations[27] and scaling as $\eta_f \sim -f^{3/2}$ for $f > 1$. Note that eqs 8 and 9 immediately imply that $\eta_1 = 0$. At the same time, it can be seen that a linear chain can be simultaneously seen as a star with $f = 1$ arm and N monomers (end-monomer representation) or as a star with $f = 2$ and $N/2$ monomers (mid-monomer representation): the partition functions $\mathcal{Z}_1(N)$ and $\mathcal{Z}_2(N/2)$ have the same N dependence.

When two stars with different functionalities, f_1 and f_2, are brought to a small separation r of the order of the monomer length a, their partition function takes the form

$$\mathcal{Z}_{f_1f_2}(r;N_1,N_2) \sim C_{f_1f_2}(r)\, \mathcal{Z}_{f_1+f_2}(N) \quad (10)$$

which reflects the fact that two stars held close together resemble a new star with functionality $f_1 + f_2$. Here N stands for either N_1 or N_2, supposing that the two are not too dissimilar, so that the radii of the two stars, which scale as N_i^ν, can be identified with a single length scale $R \sim N_i^\nu$. When $r \to \infty$, $\mathcal{Z}_{f_1f_2}(N_1,N_2)$ factorizes into the partition functions of the individual components, $\mathcal{Z}_{f_1f_2}(N_1,N_2) = \mathcal{Z}_{f_1}(N_1)\, \mathcal{Z}_{f_2}(N_2)$.

At the same time, since the monomer length scale is irrelevant for scaling arguments, the only remaining length is the aforementioned star size R. On dimensional grounds, the partition function $\mathcal{Z}_{f_1f_2}(N_1,N_2)$ must take the form

$$\mathcal{Z}_{f_1f_2}(r;N_1,N_2) \sim B_{f_1f_2}(r/R)\mathcal{Z}_{f_1}\mathcal{Z}_{f_2} \quad (11)$$

with some unknown function $B_{f_1f_2}(r/R)$. Taking into account eq 9, eqs 10 and 11 imply that

$$B_{f_1f_2}(r/R) \sim N^{-\nu\theta f_1 f_2} \quad (12)$$

with

$$\theta_{f_1f_2} = \eta_{f_1} + \eta_{f_2} - \eta_{f_1+f_2} \tag{13}$$

Taking into account the scaling $R \sim N^{\nu}$, we see that eq 12 can be fulfilled only if the function $B(z)$ is a power law of z: $B(z) \sim z^{\theta f_1 f_2}$. Finally, eq 11 is written as

$$\mathcal{Z}_{f_1f_2}(r;N_1,N_2) = \left(\frac{r}{R}\right)^{\theta f_1 f_2} \mathcal{Z}_{f_1}\mathcal{Z}_{f_2} \tag{14}$$

Combined with the definition of the effective interaction, eq 1, the last equation gives the asymptotic behavior of $V_{f_1f_2}(r)$ for small r as $\beta V_{f_1f_2}(r) \sim -\theta \ln(r/R)$. Inserting the scaling $\eta_f \sim -f^{3/2}$, we obtain therefore

$$\beta V_{f_1f_2}(r) = -\alpha[(f_1 + f_2)^{3/2} - (f_1^{3/2} + f_2^{3/2})] \ln\left(\frac{r}{R}\right) + K \tag{15}$$

with some unknown constants α and K. The constant α can be fixed by requiring that $V_{f_1f_2}$ reduces to eq 3 in the case $f_1 = f_2 = f$. Thereby, we obtain

$$\beta V_{f_1f_2}(r) = -\Theta_{f_1f_2} \ln\left(\frac{r}{R}\right) + K \tag{16}$$

where

$$\Theta_{f_1f_2} = \frac{5}{36}\frac{1}{\sqrt{2}-1}[(f_1 + f_2)^{3/2} - (f_1^{3/2} + f_2^{3/2})] \tag{17}$$

Equation 16 is the expression that we adopt for small star−chain separations, setting $f_1 = f$ and $f_2 = 2$. It remains to specify what is meant by "short". The scaling argument above holds for separations r of the order of the monomer length. However, monomers of length a can be regrouped into effective ones with increased length, $a \to \lambda a$, provided one simultaneously rescales the polymerization, $N \to \lambda^{-1/\nu}N$, thereby increasing the range of validity of the asymptotic regime. Clearly, this procedure can be carried until the rescaled monomer length has reached a size of the order of the gyration radius. We expect, thus, eq 16 to hold for $r \lesssim R$, and in the following we will test this assumption. A consequence of eq 16 is that the force $F_{cs}(r) = \hat{\mathbf{r}}\cdot\mathbf{F}_{cs}(r)$ (see eq 5) takes the form

$$\beta F_{sc}(r) = \frac{\Theta_{f_2}}{r} \tag{18}$$

implying that the inverse force scales linearly with r.

In Figure 2 we show a comparison of the results from the computer simulations and scaling theory regarding the inverse force. It can be seen that the scaling regime holds up to a separation $\sigma_{sc} = (\sigma_s + \sigma_c)/2$; i.e., the cross-diameter for the logarithmic interaction is additive. Thus, we write the star−chain effective potential as

$$\beta V_{sc}(r) = -\Theta_{f_2} \ln\left(\frac{r}{\sigma_{sc}}\right) + \bar{K} \quad \text{for } r \le \sigma_{sc} \tag{19}$$

with an additive constant $\bar{K}$ to be fixed later. It remains thus to determine the interaction in the weak overlapping regime, $r > \sigma_{sc}$.

2. The Weak Overlapping Regime. For large separations between the star center and the central monomer of the chain, we use a simple Flory-type approach, which has been shown to yield accurate results for dendritic macromolecules.[28,29] The interaction energy between the star and chain is now estimated by a simple overlap integral between the undisturbed density profiles of the two objects. This is justified, since we use this theoretic approach only for large distances, we assume that the density profiles are the profiles of the two objects for an infinite separation. Thus, $V_{sc}(r)$ reads as

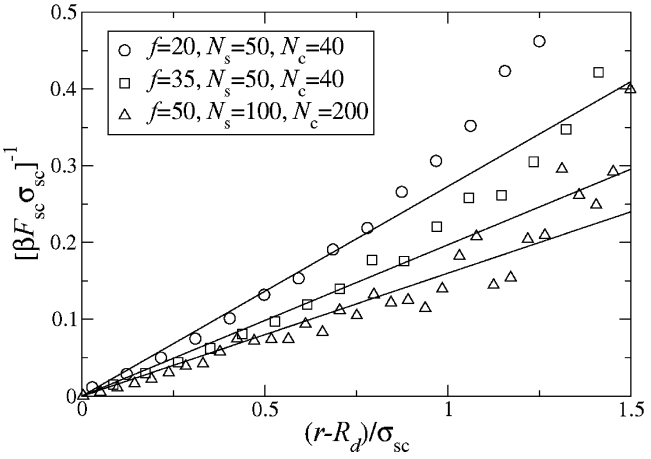

Figure 2. Inverse force $F_{cs}(r) = \hat{\mathbf{r}}\cdot\mathbf{F}_{cs}(r)$ (see eq 5) between stars of different functionalities and chains of different lengths, as indicated in the legend. The symbols denote simulation results, shifted by the star core, whereas the lines are the predictions of the theory according to eq 18. The slope in the linear part is in agreement with the theoretical description, but the scaling breaks down for separations $r > \sigma_{sc}$.

$$\beta V_{sc}(r) = \beta \int\int \mathrm{d}^3r'\, \mathrm{d}^3r''\, c_s(r')\, c_c(|\mathbf{r}'' - \mathbf{r}|) v(|\mathbf{r}' - \mathbf{r}''|) \tag{20}$$

Here, $c_s(r)$ and $c_c(r)$ are the density profiles of the star and chain, respectively, and $v(r)$ is the monomer interaction. The interaction between the monomers is approximated by a δ-function:[30−32]

$$\beta v(|\mathbf{r}' - \mathbf{r}''|) = v_0 \delta(\mathbf{r}' - \mathbf{r}'') \tag{21}$$

where v_0 has the dimension of a volume and is called excluded volume parameter. Using this interaction in eq 20, we obtain

$$\beta V(r) = v_0 \int \mathrm{d}^3r'\, c_c(r')\, c_s(|\mathbf{r}' - \mathbf{r}|) \tag{22}$$

The modeling of the density profile of the star polymers is based on the considerations in ref 20. According to the blob model of star polymers by Daoud and Cotton,[33] for sufficiently long arms the largest part of the star in good solvent conditions the monomer density follows a power law:

$$c_s(r) \sim r^{-4/3} \tag{23}$$

The length $\sigma_s/2$ is the radius from the star center up to which the scaling eq 23 holds. Outside of this region there is a layer of free rest chains. In ref 20, it was found that the local osmotic pressure in the outer region takes the form

$$\Pi(r) \propto \left(\frac{1}{r^2} + 2\kappa^2\right)\frac{\zeta}{\sigma_s} \exp\{-\kappa^2[r^2 - (\sigma_s/2)^2]\} \tag{24}$$

where κ is a fit parameter of the order $1/R_g^{(s)}$ and

$$\zeta = \frac{1}{1 + \kappa^2\sigma_s^2/2}$$

In this outer region, the monomer density is very low, and the region can be locally seen as a dilute polymer solution.

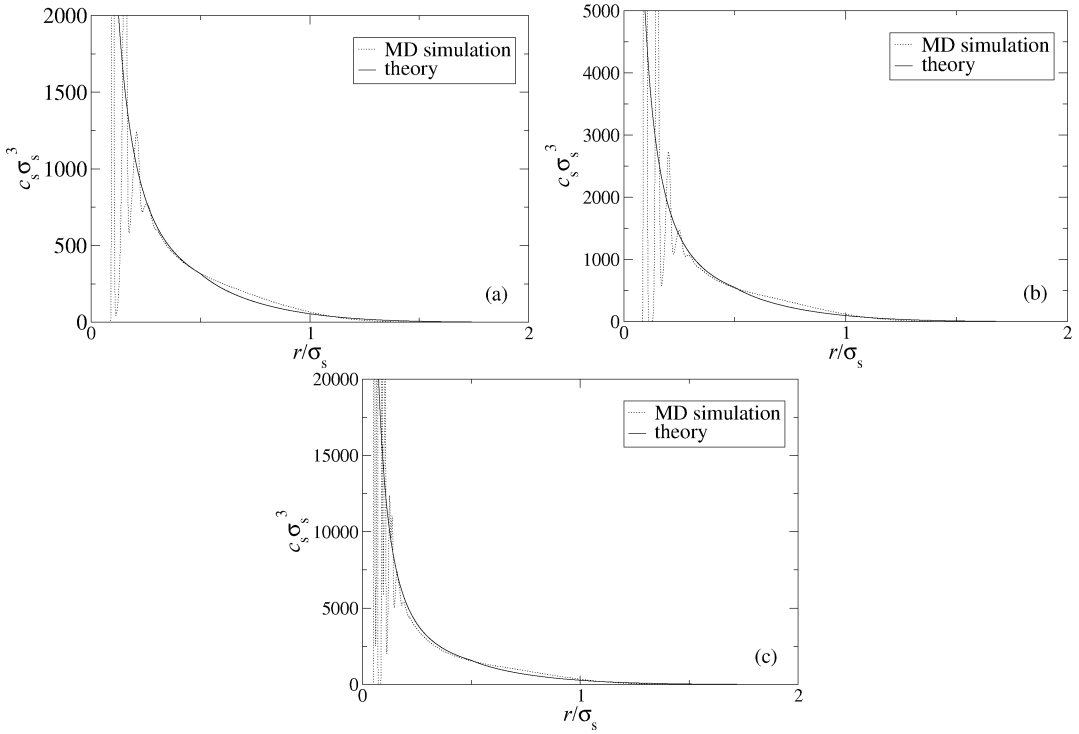

Figure 3. Monomer density profiles $c_s(r)$ of three different star polymers. Each panel shows a comparison of the simulation results and the theoretical modeling according to eq 25. (a) $f = 20$, $N_s = 50$; (b) $f = 35$, $N_s = 50$; and (c) $f = 50$, $N_s = 100$.

Therefore, $c \propto \Pi$, and the resulting density profile of a single star is then given by

$$c_s(r) = A \times \begin{cases} r^{-4/3}(\sigma_s/2)^{-5/3} & \text{for } r \le \sigma_s/2 \\ \left(\frac{1}{r^2} + 2\kappa^2\right)\frac{\zeta}{\sigma_s/2}\exp\{-\kappa^2[r^2 - (\sigma_s/2)^2]\} & \text{else} \end{cases} \quad (25)$$

The profile is continuous at $r = \sigma_s$. The prefactor A is determined by the mass conservation condition:

$$N_s f = \int \mathrm{d}^3 r\, c_s(r) \quad (26)$$

Equation 25 satisfies known conditions from scaling theory. First, since $A \propto f$ and $\sigma_s \sim af^{1/5}$, for fixed N_s, it yields $c_s(r) \propto r^{-4/3}f^{2/3}$ for $r < \sigma_s$. Subsequently, the relation $\Pi \propto c^{9/4}$ in the semidilute regime formed in the star interior yields $\Pi(r) \propto r^{-3}f^{3/2}$ there.

In Figure 3, we show a comparison between the theoretical model for the star density profiles and the simulation results. There is a single fitting parameter, namely κ which must be of the order of $1/R_g^{(s)}$. Indeed, the fit shown in Figure 3 was achieved for a value $\kappa R_g^{(s)} = 0.95$ for all three cases. Subsequently, we employ this value for all stars modeled in the theory. Apart from a region close to the grafting core, in which the local steric-induced ordering of the monomers causes oscillations in the density profile, the agreement is good. Notice, in any rate, that we are going to make use of the profiles only in their outermost domain, since the interaction for short distances is given by the scaling form, eq 19.

For the linear polymer chains, we model the profile $c_c(r)$ around the mid-monomer in the same way as for the stars, since in the inner region theory again predicts a $r^{-4/3}$ scaling,[34,35] and in the outer region we expect some exponential decay. Only the normalization condition changes and reads now as

$$N_c = \int \mathrm{d}^3 r\, c_c(r) \quad (27)$$

Again $\kappa R_g^{(c)} = 0.95$ was employed. The comparison of the model and the simulation data is shown in Figure 4.

Using these density profiles, we can now calculate effective interactions between the two macromolecular objects for $r > \sigma_{sc}$. Note that the only remaining free parameter in the theory is the excluded volume parameter v_0. This, along with the additive constant $\bar{K}$ in eq 19, is uniquely determined by the requirements that both the interaction $V_{sc}(r)$ and its first derivative with respect to r be continuous at the matching point $r = \sigma_{sc}$. The resulting values for v_0 are shown in Table 2. In Figure 5, we show the comparisons between the effective forces obtained in the MD simulations and the ones resulting from the above theoretical modeling, for which the force is given by eq 5. It can be seen that for the first three combinations there is excellent agreement between the two, whereas for the fourth one the agreement is still good. It should be pointed out, however, that for a star with $f = 100$ and $N = 50$ there is an inner region with strongly stretched monomers and that the size ratio with the associated chain is $\xi = 0.8$ (see Table 1), which is larger than the size ratios $\xi \le 0.5$ considered in this work. The agreement between theory and simulations for the parameter combinations considered gives confidence in the theoretical modeling of the profiles and the associated effective interaction.

We now need to provide a general scheme for the consistent calculation of $V_{sc}(r)$ for arbitrary functionalities f and size ratios ξ, defined as

$$\xi = \frac{\sigma_c}{\sigma_s}$$

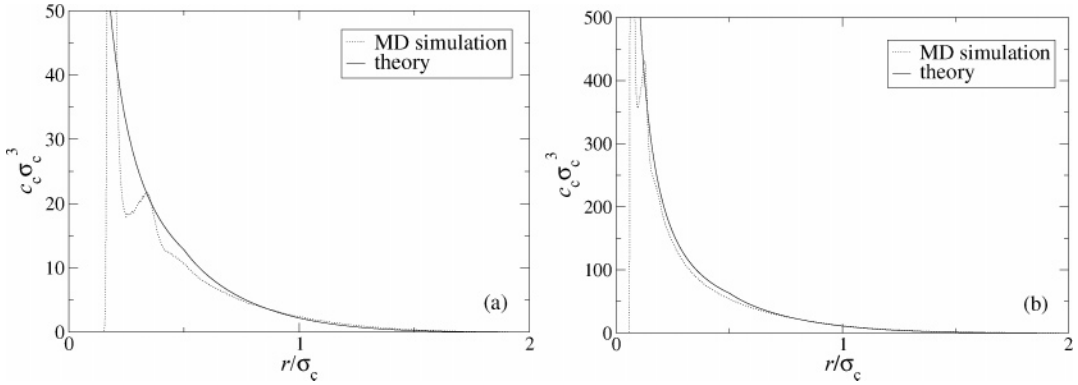

Figure 4. Monomer density profiles $c_c(r)$ of two different polymer chains. Each panel shows a comparison of the simulation results and the theoretical modeling. (a) $N_c = 40$; (b) $N_c = 200$.

Table 2. List of the Parameters of the Simulated Systems[a]

f	N_s	N_c	$v_0\sigma_{LJ}^3$
20	50	40	0.957
35	50	40	0.955
50	100	200	0.445
100	50	200	0.546

[a] The excluded volume parameter v_0 is determined by the condition that the force be continuous at $r = \sigma_{sc}$.

Here, a difficulty arises at first, since, in a mesoscopic description, the degrees of polymerization N_s and N_c of the star and the chain should drop out of sight, and they should enter the effective interactions solely through the dependence of the scales $\sigma_{s,c}$ on them, namely[30,36]

$$\sigma_s \sim f^{1/5} N_s^{3/5} \tag{28}$$

and

$$\sigma_c \sim N_c^{3/5} \tag{29}$$

At the same time, explicit values for $N_{s,c}$ are required for the normalization conditions of the density profiles. It appears that one obtains, then, different effective interactions for different $N_{s,c}$ values at fixed ξ and f. The problem, however, is only an apparent one, and it is removed because the part of the effective interaction for $r < \sigma_{sc}$ provides a strong constraint. One may choose some arbitrary (large) value for N_s and subsequently determine uniquely the corresponding value of N_c from the given size ratio ξ and eqs 28 and 29. Using these scaling relations and calculating the convolution integral from eq 22, one finds that the effective interaction $V_{sc}(r)$ in the region $r > \sigma_{sc}$ scales proportionally to $\tilde{v} = v_0 N_s^{1/5}$ and that the remaining factor depends only on the scaled separation $x = r/\sigma_{sc}$. This expression, and its derivative, have to be matched with eq 19, valid in the strong overlap region, at $x = 1$. The latter, however, depends exclusively on x, without any additional dependence on N_s. Therefore, $\tilde{v}$ turns N_s-independent. This property gives a $N_s^{-1/5}$ dependence on v_0, which shows that the latter should not be interpreted literally as the true monomer−monomer excluded volume but rather as a parameter that allows the smooth crossover from the scaling to the weak-overlapping regimes. To put it differently, one can assume just *any* degree of polymerization for the star. The scaling expression, eq 19, will then force the effective interaction to lose any explicit dependence on N_s also in the *outside* region, as long as it is expressed in terms of the scaled variable $x = r/\sigma_{sc}$, as should indeed be the case. The only dependence of the interaction on N_s and N_c comes implicitly through the dependence of the length scales σ_s, σ_c, and $\sigma_{sc} = (\sigma_s + \sigma_c)/2$ on these quantities (see eqs 28 and 29).

IV. The Many-Body Problem

Having now obtained the star−star, star−chain, and chain−chain effective interactions, we can turn our attention to finite mixture concentrations, employing for the coarse-grained description of the mixture the effective potential energy function of eq 2. The associated physical parameters are the star functionality f as well as the chain-to-star size ratio ξ; the relevant thermodynamic parameters are the two partial densities $\rho_\alpha = \mathcal{N}_\alpha/\Omega$, α = c,s, where $\mathcal{N}_{c,s}$ denote the numbers of stars and chains, respectively, enclosed in the macroscopic volume Ω. For the calculation of the pair structure, the sought-for quantities are the corresponding partial distribution functions $g_{\alpha\beta}(r)$ or, equivalently, the partial structure factors $S_{\alpha\beta}(k)$, defined as[37]

$$S_{\alpha\beta}(k) = \delta_{\alpha\beta} + \sqrt{\rho_\alpha \rho_\beta} \int \mathrm{d}^3 r\, [g_{\alpha\beta}(r) - 1] \exp(-\mathrm{i}\mathbf{k}\cdot\mathbf{r}) \tag{30}$$

The distribution functions have been calculated by employing standard tools from integral equation theory. In particular, we solved the two-component Ornstein−Zernike equation[7,37] complemented with the Rogers−Young closure.[38]

A. Mixtures at Low Star Concentrations. *1. Chain-Modified Star−Star Interaction.* We can make one more step in the coarse-graining process and integrate out the linear chains, describing thereby the system as an effective, one-component star solution. In this way, the star−star interaction $V_{ss}(r)$ gets renormalized, and a higher-level effective interaction between the stars, $V_{eff}(r)$, arises, which depends on f, size ratio, and, most importantly, the chain concentration ρ_c. In this way, we can gain insight into the ways of modifying the behavior of a concentrated star solution by changing any of the above characteristics of the linear additives. The quantity $V_{eff}(r)$ can be obtained within the framework of two-component integral equations. Starting from the radial distribution function in the limit of infinite dilution of star polymers, the effective interaction between them in the presence of polymer chains is given by[39]

$$V_{eff}(r; \rho_c) = -\lim_{\rho_s \to 0} \ln g_{ss}(r; \rho_s, \rho_c) \tag{31}$$

and depends parametrically on the (reservoir) density of the linear chains.

In Figure 6, we show the dependence of the effective interaction on the properties of the added polymer, taking now a typical experimental functionality $f = 73$ as a representative.

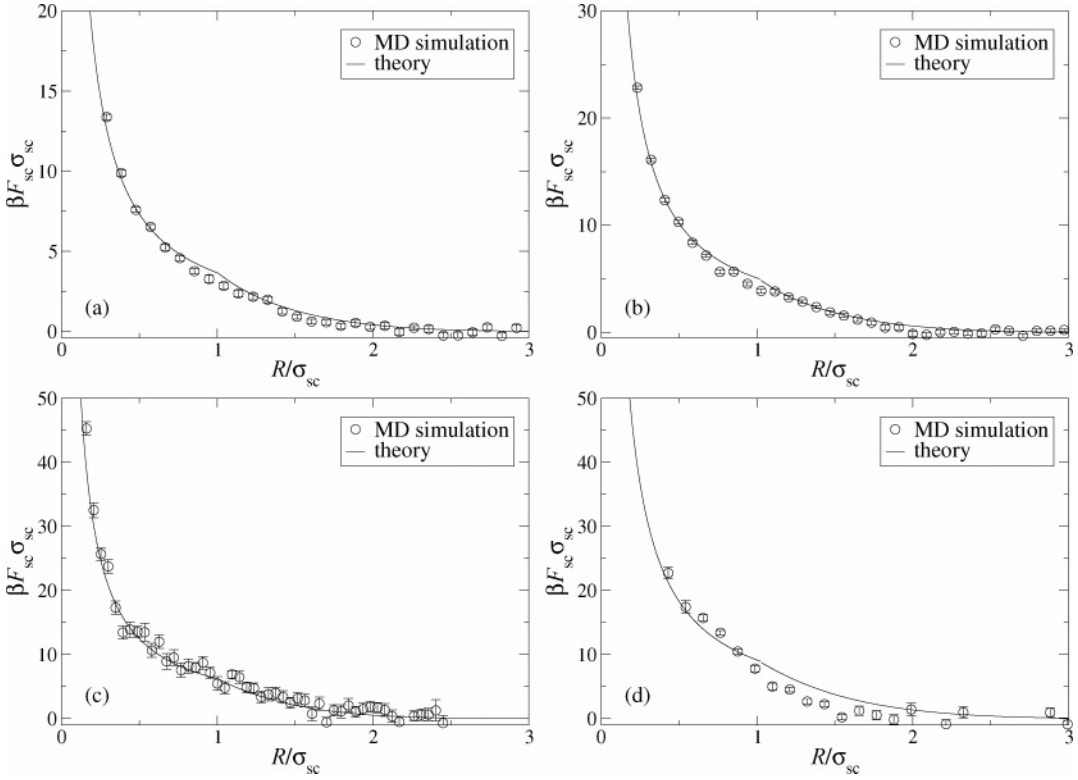

Figure 5. Mean force between the star and chain as a function of the distance of the star and chain center. The circles denote the simulation results, and the solid line denotes the results from the theoretic modeling. The force is calculated for (a) $f = 20$, $N_s = 50$, $N_c = 40$; (b) $f = 35$, $N_s = 50$, $N_c = 40$; (c) $f = 50$, $N_s = 100$, $N_c = 200$; and (d) $f = 100$, $N_s = 50$, $N_c = 200$.

It is instructive to see how different the effect of the linear additives is depending on the size ratio ξ. For $\xi = 0.1$ (Figure 6a), the addition of polymer chains leads first to a weakening of the repulsion between the stars, until a strong depletion attraction is induced. Notice that the chain density in the legend is expressed in units of the chain size; it lies well below its overlap value, but it is nevertheless large when expressed in units of the star size, as it gets multiplied by a factor ξ^{-3}. A attractive part develops, which is due to the osmotic pressure of the many small chains pushing the two stars together, a *depletion* phenomenon well-known also from the case of colloid−polymer mixture. This attraction is devoid of any significant secondary maximum (hump) at larger separations and can lead to a star−chain demixing transition. In the intermediate region of size ratios, $\xi = 0.3$, shown in Figure 6b, the resulting interaction displays a competition of short-range attractions and long-range repulsions, which lead to the formation of finite equilibrium clusters, to be discussed below. Here, the presence of the repulsive hump plays the decisive role in stabilizing the multistar aggregates.[24,25]

An unusual feature develops for the case of the largest size ratio considered, $\xi = 0.5$, shown in Figure 6c. The chains bring about no attraction between the stars, only a reduction of the repulsion range. The striking effect, however, lies in the fact that beyond the overlap density of the chains, $\rho_c^* \sigma_c^3 \approx 1$, the interaction remains virtually unchanged by the addition of more chains. The phenomenon is unknown for the usual cases of colloid−polymer or colloid−colloid depletion, for which the effective potential has a strong dependence on the depletant density.[7] Here, it seems that the effect of the chains saturates when they reach their overlap density and that this feature is present only when the chains have a size comparable to that of the stars. The novelty arises from the soft nature of the cross-interaction potential, $V_{sc}(r)$, as opposed to the hard interactions encountered in colloid mixtures and can be traced back to the increased penetration of the chains into the stars as their density grows.

To provide an independent check on this phenomenon and to understand better the role of the penetrability, we have calculated the depletion force between the stars using an alternative approach, the superposition approximation.[40] The geometry is shown in Figure 7. Let the star on the left be placed at the origin and a second star be at separation **r** from the first. The two are immersed in a solution of linear chains, and the local chain density at position **s** is $\rho_c(\mathbf{s};\mathbf{r})$, depending parametrically on the star−star separation. We consider the chain-mediated force acting on the star at the origin, which we call depletion force, $\mathbf{F}_{dep}(r)$; it is positive if it repels the two stars and negative otherwise. With this convention, we consider now the quantity $F_{dep}(r) = -\hat{\mathbf{r}}\cdot\mathbf{F}_{dep}(r)$, which is given by

$$F_{dep}(r) = -2\pi \int_0^\infty r^2 \frac{dV_{sc}(r)}{dr} \int_{-1}^{1} \rho_c(\mathbf{r};\mathbf{R}_1,\mathbf{R}_2)\omega \, d\omega \, dr \tag{32}$$

where $\omega = \cos\theta$. In the superposition approximation, the chain density $\rho_c(\mathbf{s};\mathbf{r})$ is decomposed as a product of the radial distributions of two isolated stars, shifted by the distance **r**, i.e.

$$\rho_c(\mathbf{s};\mathbf{r}) = \rho_c g_{sc}(s)\, g_{sc}(|\mathbf{s} - \mathbf{r}|) \tag{33}$$

With this approximation we obtain

$$F_{dep}(r) = -2\pi \int_0^\infty h(r,s)\, ds \tag{34}$$

where

$$h(r,s) = \rho_c s^2 \frac{dV_{sc}(s)}{ds} g_{sc}(s)\, f(r,s) \tag{35}$$

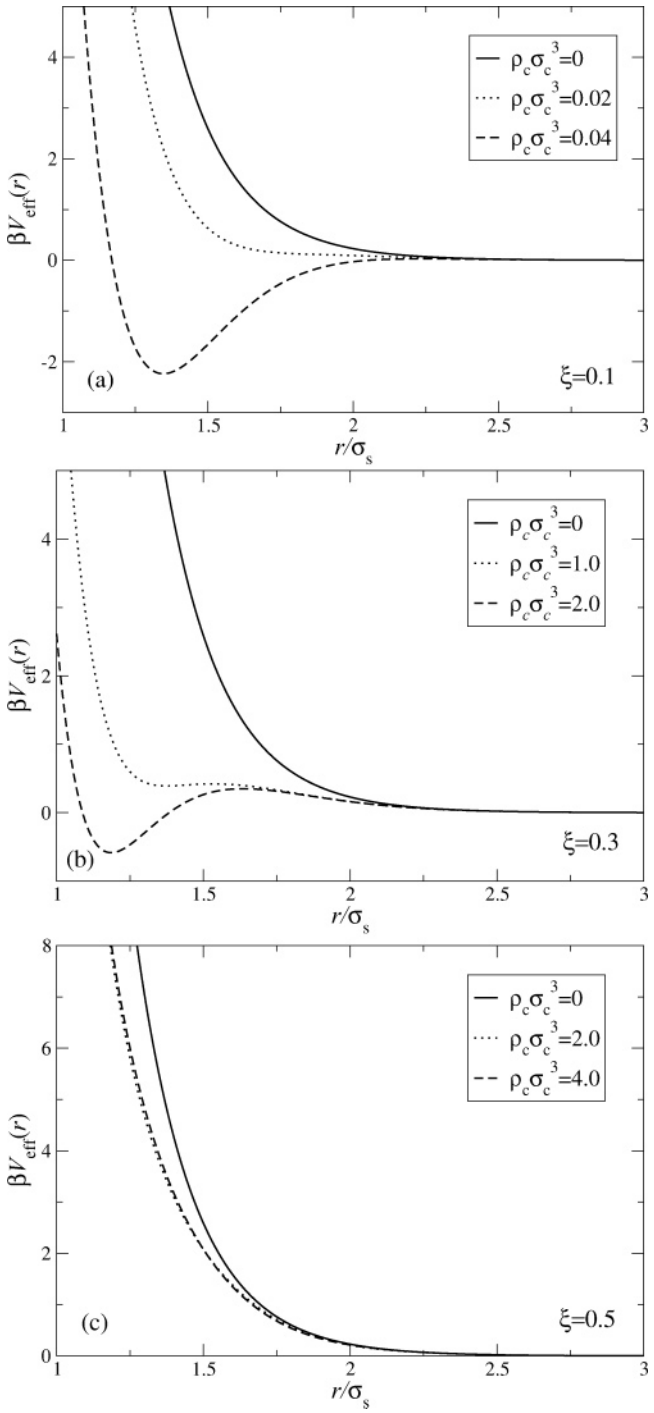

Figure 6. Effective interaction between the stars modified by the presence of the chains. The functionality is $f = 73$ in all cases; the size ratio is indicated in the figure.

and

$$f(r,s) = \int_{-1}^{1} g_{sc}\left(\sqrt{r^2 + s^2 - 2rs\omega}\right)\omega \, d\omega \qquad (36)$$

In Figure 8, we show the individual terms that are involved in $F_{dep}(r)$, in order to gain some insight into the mechanism that leads to the insensitivity of the depletion force and thus of the effective one, since the latter is the sum of the depletion force and the direct star−star force. When functions of the two variables r and s are shown, we fix the interstar separation to the value $r = 1.5\sigma_s$, for which, according to Figure 6c, $V_{eff}(r)$ hardly changes with ρ_c, and we plot the functions against the integration variable s.

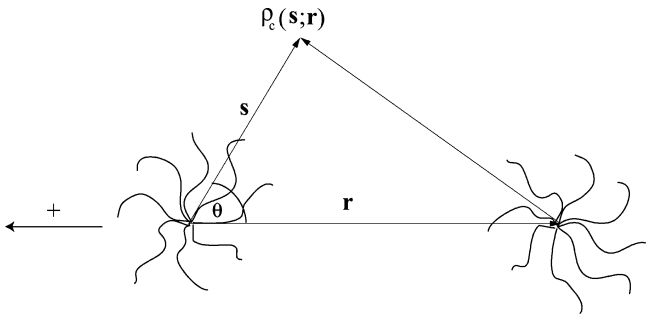

Figure 7. Geometry of two stars, separated by the vector **r** and being immersed in a sea of linear chains (not drawn). The star on the left is positioned at the origin. At the point described by the position vector **s**, the chain density is $\rho_c(\mathbf{s};\mathbf{r})$, where the second argument indicates its dependence on the star separation **r**. The arrow denotes the direction along which the effective force acting on the star on the left is chosen as positive.

The angularly averaged radial distribution $f(r = 1.5\sigma_s, s)$ (Figure 8b) is strongly dependent on depletant density. Interestingly, though, it is most negative for the lowest density, and its magnitude decreases for increasing density. The reason for this behavior lies in the penetrability of $g_{sc}(r)$ shown in Figure 8a. Because of the additional presence of the ω-term in the integrand, the function $f(r,s)$ would vanish identically if the function $g_{sc}(z)$ were equal to unity for all z. An increase in ρ_c and the concomitant penetration inside the soft core pushes g_{sc} precisely in this direction and causes $f(r,s)$ to decrease in magnitude.

This decrease is compensated again upon multiplication with ρ_c and $g_{sc}(s)$, which yield the function $h(r,s)$ (eq 35) shown in Figure 8c. Indeed, the three curves for the three different densities integrate to very similar values. Again, a partial role is played by the multiplication of $f(r,s)$ with $g_{sc}(s)$, which penetrates deeper into the star when ρ_c increases without developing any pronounced correlation structure. These are the signatures of the ultrasoft cross-interactions; thus, this phenomenon is absent for the depletion force between impenetrable colloids. Finally, in Figure 8d, we show the resulting depletion force from the superposition approximation. In full consistency with the results from the inversion of $g_{ss}(r;\rho_s,\rho_c)$ (eq 31), there is hardly any variation with ρ_c for $r \gtrsim 1.5\sigma_s$ when $\rho_c\sigma_c^3 \gtrsim 1$. Note that the depletion force *does* change with ρ_c for smaller separations, yet this effect is masked by the direct force $F_{ss}(r) = -dV_{ss}(r)/dr$, which is much larger in magnitude than the depletion force at such length scales.

It is tempting to associate this phenomenon with a worsening of solvent quality for the stars as chains are added. Once the latter have reached and exceeded their overlap concentration, the solvent has reached the vicinity of the Θ-point, and hence the stars feel the effective interaction akin to Θ-like conditions. Further increase of the chain concentration within the semidilute regime does not bring about any additional change of solvent quality; hence, the effective interaction does not change anymore. It is intriguing that the coarse-grained description may be able to reproduce such a behavior, and further investigations are needed to explore a possible deeper connection with the classical theory of polymers. Our findings may explain, however, the experimentally observed insensitivity of the behavior of star polymer gels upon addition of linear chains, when the chain−star size ratio exceeds, roughly, the value 0.5 (see ref 23).

2. Cluster Formation. An interesting phenomenon taking place in star−linear mixtures at very low concentrations is that of cluster formation between the stars, when the added chains approach or exceed their overlap concentration.[24,25] This has

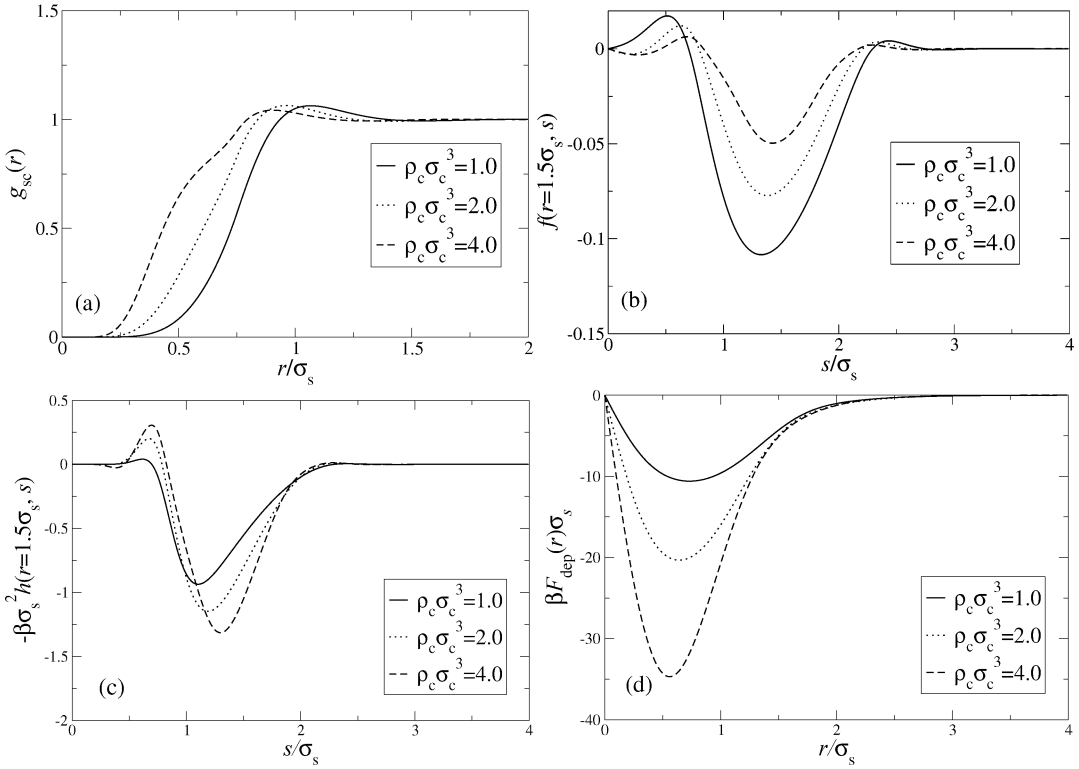

Figure 8. (a) Star−linear cross-distribution function $g_{sc}(r)$ for $f = 73$, $\xi = 0.5$, star density $\rho_s = 0$, and chain densities as indicated in the legend. (b) Function $f(r;s)$ of eq 36 at $r = 1.5\sigma_s$. (c) Function $\rho_c h(r,s)$ defined in eq 35 for $r = 1.5\sigma_s$. (d) Full depletion force in the superposition approximation. Note the insensitivity to ρ_c for $r > 1.5\sigma_s$.

been experimentally documented by a sudden increase of the measured hydrodynamic radius of the stars at the overlap concentration of the chains, by as much as an order of magnitude. Clearly, the measured hydrodynamic radius is not that of a single star, but it corresponds rather to a clump (cluster) formed by many stars and stabilized by the presence of the chains. The conditions under which equilibrium clusters form in soft-matter systems have been the subject of intensive investigations recently.[24,25,41−47]

The current understanding of the mechanism that drives the formation of stable, equilibrium cluster rests on the role played by the existence, in the effective interaction, of a short-range attractive well followed by a long-range repulsive hump. Although extremely short-range attractions and long-range repulsions were initially employed,[41−43] it has been shown that also moderate values of the same can lead to the formation of clusters.[24,25,44−46] Moreover, the interaction at short particle overlaps need not be hard; even the soft star−polymer type interactions are sufficient.[44] The attractions can even be dropped, and still clusters will form if the repulsion is ultrasoft, allowing full particle overlaps and decaying sufficiently fast to zero at large separations.[48]

Here, we employ the accurate cross-interaction $V_{sc}(r)$ along with the other two interactions, $V_{ss}(r)$ and $V_{cc}(r)$, to investigate the existence and stability of star clusters due to the added chains. In this way, we improve over previous studies that employed a heuristic cross-interaction in the center-of-mass representation.[24,25] In order to investigate cluster formation, we examine the star−star structure factor of the system. We probe the dependence of the cluster formation on the star functionality and the size ratio between the star and the added polymer. The presence of clusters is signaled by the appearance in the star−star structure factor of a new length scale that is larger than the typical star−star separation $a_s = \rho_s^{-1/3}$.

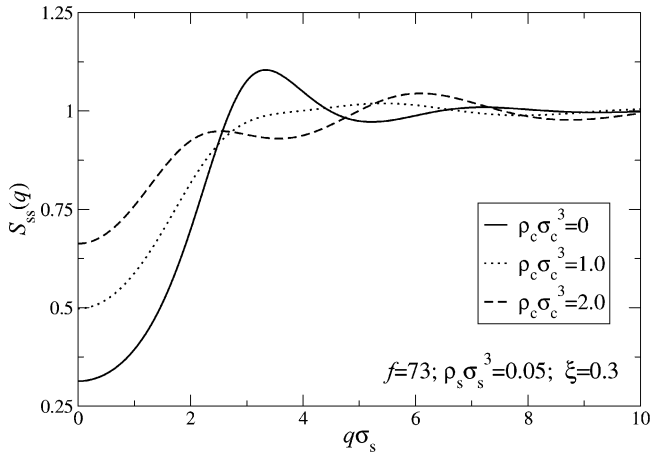

Figure 9. Star−star structure factor $S_{ss}(q)$ at different chain concentrations for star functionality $f = 73$. The star number density is kept constant at $\rho_s\sigma_c^3 = 0.05$.

In Figure 9, we show the development of the structure factor at *fixed* star density $\rho_s\sigma_s^3 = 0.05$ on increasing the chain concentration for star functionality $f = 73$ and chain-to-star size ratio $\xi = 0.3$. Upon increasing ρ_c, the peak height first decreases and shifts to larger q, then the peak splits, and a new peak at small q appears. The length scale which is associated with this value is much larger than the size of the individual stars; therefore, we associate this length scale with the formation of equilibrium clusters in the system. Eventually, for even higher chain concentrations, the maximum in the structure factor will shift to $q = 0$, signaling the approach of a macroscopic phase separation for large polymer densities. Note that the equilibrium clusters, as signaled by the development of a prepeak in the star−star structure factor, appear when the chains reach their overlap concentration, in agreement with experimental measure-

ments.[25] The organization of the stars into aggregates is in agreement with the characteristics of the effective star−star interaction shown in Figure 6b. Indeed, for this particular size ratio, $\xi = 0.3$, $V_{\text{eff}}(r)$ displays a short-range attraction, followed by a repulsive hump. The rather weak prepeak in the structure factor points to the existence of fluctuating clusters, which exchange particles, as opposed to a cluster phase with tightly bounded supramolecular aggregates. For small size ratios, e.g., $\xi = 0.1$, the effective interaction is devoid of a repulsive hump (see Figure 6a), and thus the system is driven into macrophase separation that is not preceded by the appearance of stable clusters with a well-defined size. For higher ξ values, the chains do not induce any attraction between the stars (see Figure 6c); thus, again no clusters appear. These facts demonstrate that cluster formation is very sensitive on the physical characteristics of the constituents and can be steered by external control of the size ratio, for instance.

B. Mixtures for High Star Concentrations. Finally, here we turn our attention to a physical situation that is specular to the one discussed in the preceding subsection, namely high star concentration and low chain concentration. Also in this case, the chains can have a dramatic impact in the behavior of the dense star solution. It is known that high functionality star polymers undergo a dynamical arrest transition at a certain critical density ρ_s^{cr}, roughly at $\rho_s^{cr}\sigma_s^3 \cong 0.4$. This structural arrest, seen in rheological[5,49,50] and light scattering experiments,[24] has also been investigated theoretically within the framework of mode-coupling theory[51] (MCT) based on the interaction potential $V_{ss}(r)$. The arrest can be identified with a glass transition that arises from the mutual repulsions between stars that lead to caging. Accordingly, it is absent for functionalities $f \lesssim 50$, for which the interstar repulsion of eq 3 is not strong enough to sustain self-supporting cages.

The influence of multistar additives on this soft colloidal glass has been investigated for binary star polymer mixtures.[52] As far as the effect of linear additives is concerned, experimental studies of star polymer−linear chains mixture find a chain induced melting of the star polymer glass, which is caused by a softening of the star−star repulsion.[23] Here, we investigate the phenomenon applying the accurate cross-interaction potential $V_{sc}(r)$. Already the information encoded in Figure 6 points to the fact that the additives should have the effect of melting the star glass. Indeed, they bring about invariably a reduction of the interstar repulsion due to a classical depletion effect. In this way, the stars, in the presence of the linear polymer, become more penetrable, and this leads to a reduction of the interstar correlations and a reduction of the peak height in the star−star structure factor $S_{ss}(q)$. This can be seen in the main plot of Figure 10, which shows a characteristic example for $S_{ss}(q)$ of $f = 122$-arm stars at density $\rho_s\sigma_s^3 = 0.4$ lightly above the critical glass concentration. There is a small reduction of the peak height upon addition of chains, which is nevertheless sufficient to cause restoration of ergodicity, since we are right at the brink of the ergodic-to-nonergodic transition.

To study the dynamics and vitrification in this system, we employ ideal mode coupling theory.[53,54] Assuming that the polymer remains mobile in the mixture, we can base our analysis on one-component MCT, using only the structure factors of the stars as input.[52,55] The object of main interest from MCT is the star−star nonergodicity factor $f_{ss}(q)$, which expresses the $t \rightarrow \infty$ limit of the density time-autocorrelation function. Thus, $f_{ss}(q) = 0$ for an ergodic state in which all density fluctuations decay exponentially in time, but $f_{ss}(q) \neq 0$ for an ideal glass. The inset of Figure 10 shows the evolution of the nonergodicity

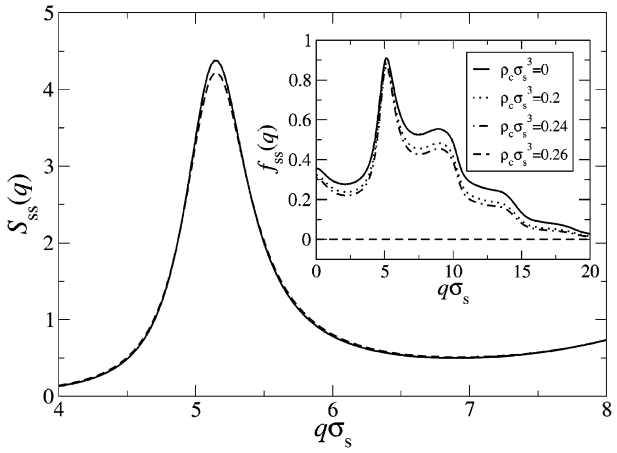

Figure 10. Main plot: the star−star structure factor for $f = 122$-arm stars at density $\rho_s\sigma_s^3 = 0.4$. Solid line: no added chains, $\rho_c\sigma_c^3 = 0$. Dashed line: with added chains of size ratio $\xi = 0.3$ and density $\rho_c\sigma_c^3 = 0.26$. Note the small but clear decrease of the height of the main peak. Inset: the star−star nonergodicity factor $f_{ss}(q)$ for the same mixture, at fixed star concentration $\rho_s\sigma_s^3 = 0.4$ and increasing chain density as indicated in the legend. Below the threshold value $\rho_c\sigma_c^3 = 0.26$, the nonergodicity factor is finite, corresponding to an arrested state, whereas at $\rho_c\sigma_c^3 = 0.26$, $f_{ss}(q) = 0$, denoting restoration of ergodicity.

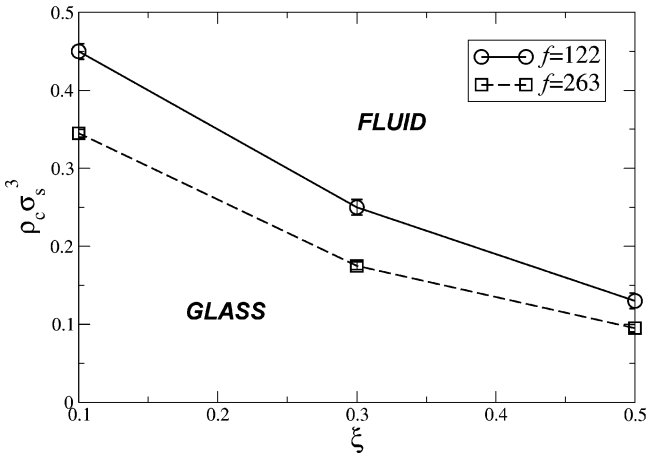

Figure 11. Ideal MCT transition lines for star polymers with $f = 122$ and $f = 263$. Here, the star densities are fixed at $\rho_s\sigma_s^3 = 0.4$ for $f = 122$ and $\rho_s\sigma_s^3 = 0.35$ for $f = 263$. The points denote the density of chains that is needed to reach the nonergodic-to-ergodic transition as a function of the size ratio. The lines are a guide to the eye. Above the line corresponding to each f the system is fluid and below glassy.

factor upon addition of chains and manifests the transition from a glassy to an ergodic state at some critical chain concentration. A compilation of MCT results for various parameter combinations is finally show in Figure 11. This represents a kinetic phase diagram of the system, as obtained by ideal MCT, and again manifests the influence of the composition of the mixture on the dynamics of the system. The basic trends are in agreement with the experimental findings in ref 23 as well as comparable to the behavior for binary star polymer mixtures when the small component remains mobile in the matrix formed by the big one.[52] The chain number density required to melt the glass decreases with increasing size ratio ξ. The glass melting of the stars can be interpreted as a worsening of the solvent quality for the stars upon addition of the chains.[57]

V. Conclusions

We have derived accurate effective interactions between star polymers of functionality f and linear homopolymer chains. The

latter have been coarse-grained in the mid-monomer representation, a choice that renders them equivalent to $f = 2$ stars with half the degree of polymerization per arm. Together with the previously derived star−star and chain−chain interactions, this allows for a full, coarse-grained description of star−linear polymer mixtures and the calculation of the static pair structure of the system. To the extent that statics dictates also dynamical arrest, as in the case of the MCT scenario for the glass transition, the coarse-grained description also allows for predictions regarding the rheological state of the mixture and the influence of the chains on the flow of the stars. We have confirmed a host of phenomena observed experimentally, such as cluster formation and glass melting, by using this accurate representation. It is rewarding that this approach does not alter the results obtained previously, when the chains were coarse-grained in the center-of-mass representation and a more empirical form of the cross-interaction was used.[23,25] In this respect, the results of this work are compatible with the requirement that the choice of the effective coordinates should not alter the physics of the problem at hand, although, of course, it alters the form of the effective interactions employed. The equivalence of the physical results is only guaranteed, however, when the employed effective interactions do not involve too drastic approximations, i.e., when they capture the physics of the system correctly. A similar equivalence of the center-of-mass vs mid-monomer representations was recently established for colloid−polymer mixtures.[56]

A very useful tool that arises out of a second coarse-graining procedure is the chain-modified star−star effective interaction potential. In this work, we established that the form of the latter strongly depends on size ratio. It can feature attractive wells with or without subsequent repulsive humps, or it can differ only slightly from the bare star−star interaction as the size ratio grows. The present work dealt with good and athermal solvents. A question of great interest is the coarse-grained description of star−linear mixtures in marginal or even Θ-solvents. Experimental results on such systems suggest that, once more, the size ratio of the mixture plays a crucial role.[57] For small size ratios, the chains penetrate into the innermost part of the stars, thereby effectively improving solvent quality, an effect opposite to that in good solvents. For large size ratios, however, the chains cause star shrinking.[57] It is a challenging task to attempt a coarse-graining procedure for the case of marginal solvents and to investigate the systematic differences with the good-solvent effective interactions and their ability to describe the experimental findings of ref 57.

Acknowledgment. The authors thank Martin Konieczny, Arben Jusufi, Emanuela Zaccarelli, Andrew Archer, and Roland Roth for helpful discussions. C.M. has been supported by the Düsseldorf Entrepeneurs Foundation.

References and Notes

(1) See, e.g.: Poon, W. C. K. *J. Phys.: Condens. Matter* **2002**, *14*, R859 and references therein.
(2) Sciortino, F.; Tartaglia, P. *Adv. Phys.* **2005**, *54*, 471.
(3) Bolhuis, P. G.; Louis, A. A.; Hansen, J.-P. *Phys. Rev. Lett.* **2002**, *89*, 128302.
(4) Allahyarov, E.; Löwen, H. Louis, A. A.; Roth, R. *Phys. Rev. E* **2002**, *65*, 061407.
(5) Vlassopoulos, D.; Fytas, G.; Pakula, T.; Roovers, J. *J. Phys.: Condens. Matter* **2001**, *13*, R855.
(6) Likos, C. N. *Soft Matter* **2006**, *2*, 478.
(7) Likos, C. N. *Phys. Rep.* **2001**, *348*, 261.
(8) Witten, T. A.; Pincus, P. A. *Macromolecules* **1986**, *19*, 2509.
(9) Likos, C. N.; Löwen, H.; Watzlawek, M.; Abbas, B.; Juckniscke, O.; Allgaier, J.; Richter, D. *Phys. Rev. Lett.* **1998**, *80*, 4450.
(10) Laurati, M.; Stellbrink, J.; Lund, R.; Richter, D.; Zaccarelli, E. *Phys. Rev. Lett.* **2005**, *94*, 195504.
(11) Jusufi, A.; Watzlawek, M.; Löwen, H. *Macromolecules* **1999**, *32*, 4470.
(12) Krüger, B.; Schäfer, A. Baumgärtner, J. *J. Phys. (Paris)* **1989**, *50*, 3191.
(13) Grest, G. S.; Kremer, K. *Phys. Rev. A* **1986**, *33*, 3628.
(14) Olaj, O. F.; Landschbauer, W.; Pelinka, H. *Macromolecules* **1980**, *13*, 299.
(15) Olaj, O. F.; Zifferer, G.; Rehmann, H. *Monatsh. Chem.* **1985**, *116*, 1395.
(16) Grosberg, A. Y.; Khalatur, A. R.; Khokhlov, A. R. *Makromol. Chem., Rapid Commun.* **1982**, *3*, 709.
(17) Schäfer, L.; Baumgärtner, A. *J. Phys. (Paris)* **1986**, *47*, 1431.
(18) Dautenhahn, J.; Hall, C. K. *Macromolecules* **1994**, *27*, 5933.
(19) Louis, A. A.; Bolhuis, P. G.; Hansen, J.-P.; Meijer, E.-J. *Phys. Rev. Lett.* **2000**, *85*, 2522.
(20) Jusufi, A.; Dzubiella, J.; Likos, C. N.; von Ferber, C.; Löwen, H. *J. Phys.: Condens. Matter* **2001**, *13*, 6177.
(21) Grest, G. S.; Kremer, K.; Witten, T. A. *Macromolecules* **1987**, *20*, 1376.
(22) Grest, G. S.; Kremer, K. *Phys. Rev. A* **1986**, *33*, 3628.
(23) Stiakakis, E.; Vlassopoulos, D.; Likos, C. N.; Roovers, J.; Meier, G. *Phys. Rev. Lett.* **2002**, *89*, 208302.
(24) Stiakakis, E.; Petekidis, G.; Vlassopoulos, D.; Likos, C. N.; Iatrou, H.; Hadjichristidis, N.; Roovers, J. *Europhys. Lett.* **2005**, *72*, 664.
(25) Likos, C. N.; Mayer, C.; Stiakakis, E.; Petekidis, G. *J. Phys.: Condens. Matter* **2005**, *17*, 3379.
(26) von Ferber, C.; Jusufi, A.; Watzlawek, M.; Likos, C. N.; Löwen, H. *Phys. Rev. E* **2000**, *62*, 6949.
(27) Batoulis, J.; Kremer, K. *Macromolecules* **1989**, *22*, 4277.
(28) Likos, C. N.; Schmidt, M.; Löwen, H.; Ballauff, M.; Pötschke, D.; Lindner, P. *Macromolecules* **2001**, *34*, 2914.
(29) Likos, C. N.; Rosenfeldt, S.; Dingenouts, N. Ballauff, M.; Lindner, P.; Werner, N.; Vögtle, F. *J. Chem. Phys.* **2002**, *117*, 1869.
(30) Doi, M.; Edwards, S. F. *The Theory of Polymer Dynamics*; Clarendon Press: Oxford, 1986.
(31) Stockmayer, W. H. *Makromol. Chem.* **1960**, *35*, 54.
(32) Zimm, B. H.; Stockmayer, W. H.; Fixman, M. *J. Chem. Phys.* **1953**, *22*, 1716.
(33) Daoud, M.; Cotton, J. P. *J. Phys. (Paris)* **1982**, *43*, 531.
(34) Daoud, M.; Cotton, J. P.; Farnoux, B.; Jannink, G.; Sarma, G.; Benoit, H.; Duplessix, R.; de Gennes, P. G. *Macromolecules* **1985**, *8*, 804.
(35) Edwards, S. F. *Proc. R. Soc. London* **1965**, *85*, 613.
(36) Grest, G. S.; Fetters, L. J.; Huang, J. S.; Richter, D. *Adv. Chem. Phys.* **1996**, *XCIV*, 67.
(37) Hansen, J.-P.; MacDonald, I. R. *Theory of Simple Liquids*, 3rd ed.; Academic: London, 2006.
(38) Rogers, F. J.; Young, D. A. *Phys. Rev. A* **1984**, *30*, 999.
(39) Dzubiella, J.; Likos, C. N.; Löwen, H. *J. Chem. Phys.* **2002**, *116*, 9518.
(40) Attard, P. *J. Chem. Phys.* **1989**, *91*, 3083.
(41) Mossa, S.; Sciortino, F.; Tartaglia, P.; Zaccarelli, E. *Langmuir* **2004**, *20*, 10756.
(42) Sciortino, F.; Mossa, S.; Zaccarelli, E.; Tartaglia, P. *Phys. Rev. Lett.* **2004**, *93*, 055701.
(43) Liu, Y.; Chen, W.-R.; Chen, S.-H. *J. Chem. Phys.* **2005**, *122*, 044507.
(44) Lo Verso, F.; Likos, C. N.; Reatto, L. *Prog. Colloid Polym. Sci.* **2006**, *133*, 78.
(45) Imperio, A.; Reatto, L. *J. Phys.: Condens. Matter* **2004**, *16*, 3769.
(46) Imperio, A.; Reatto, L. *J. Chem. Phys.* **2006**, *124*, 164712.
(47) Stradner, A.; Sedgwick, H.; Cardinaux, F.; Poon, W. C. K.; Egelhaaf, S. U.; Schurtenberger, P. *Nature (London)* **2004**, *432*, 492.
(48) Mladek, B. M.; Gottwald, D.; Kahl, G.; Neumann, M.; Likos, C. N. *Phys. Rev. Lett.* **2006**, *96*, 045701.
(49) Kapnistos, M.; Vlassopoulos, D.; Fytas, G.; Mortensen, K.; Fleischer, G.; Roovers, J. *Phys. Rev. Lett.* **2000**, *85*, 4072.
(50) Loppinet, B.; Stiakakis, E.; Vlassopoulos, D.; Fytas, G.; Roovers, J. *Macromolecules* **2001**, *34*, 8216.
(51) Foffi, G.; Sciortino, F.; Tartaglia, P.; Zaccarelli, Lo Verso, F.; Reatto, L.; Dawson, K. A.; Likos, C. N. *Phys. Rev. Lett.* **2002**, *90*, 238301.
(52) Zaccarelli, E.; Mayer, C.; Asteriadi, A.; Likos, C. N.; Sciortino, F.; Roovers, J.; Iatrou, H.; Hadjichristidis, N. Tartagila, P.; Löwen, H.; Vlassopoulos, D. *Phys. Rev. Lett.* **2005**, *95*, 268301.
(53) Götze, W. In *Liquids, Freezing and Glass Transition*; Hansen, J.-P., Levesque, D., Zinn-Justin, J., Eds.; North-Holland: Amsterdam, 1991; p 287.
(54) Binder, K.; Kob, W. *Glassy Materials and Disordered Solids*; World Scientific: Singapore, 2005.
(55) Zaccarelli, E.; Löwen, H.; Wessels, P. P. F.; Sciortino, F.; Tartaglia, P.; Likos, C. N. *Phys. Rev. Lett.* **2004**, *92*, 225703.
(56) Vink, R. L. C.; Jusufi, A.; Dzubiella, J.; Likos, C. N. *Phys. Rev. E* **2005**, *72*, 030401(R).
(57) Stiakakis, E.; Vlassopoulos, D.; Roovers, J. *Langmuir* **2003**, *19*, 6645.

MA062117Z